Paper No. 1157. (quote when citing this article)
Eleventh World Conference on Earthquake Engineering
ISBN: 0 08 042822 3

SIMPLIFIED TIME-DOMAIN EXPRESSIONS FOR POROUS SOIL-STRUCTURE INTERACTION

Xiu LUO*, Kazuo KONAGAI*, Assadollah NOORZAD**, Toyoaki NOGAMI***

*Institute of Industrial Science, University of Tokyo
7-22-1, Roppongi, Minato-ku,Tokyo 106, Japan

**Dept. of Civil Engineering, Tehran University
PO BOX, 11365-4563, Tehran, Iran

***Dept. of Civil and Environmental Engineering, University of Cincinnati
PO BOX, 210071, Cincinnati, OH 45221, USA

ABSTRACT

In studying soil-structure interaction, extracting typical features of wave radiation would provide important clues to simplify the expression of soil reactions to the motion of the foundation of interest. In the present approach, the porous soil surrounding a foundation is sliced into a number of elements taking into account various wave radiation patterns. The soil impedance functions for various vibration modes are then well approximated by syntheses of springs and dashopts which are not dependent on the excitement frequency at all, but the functions of equivalent Poisson' s ratio, thus, allowing time-domain analysis to be easily conducted. It is found possible for the equivalent Poisson' s ratio to be quite different from the one obtained through the in-situ PS logging, depending on the bulk moduli of the solid and liquid phases and the permeability of soil. The effect of these parameters is examined by analyzing the response of an upright Timoshenko beam with the present soil models attached.

KEYWORDS

Porous soil-structure Interaction; Embedded foundation; Time-domain analysis; Biot' s theory

INTRODUCTION

In dealing with a soil-structure interaction problem, one of the key tasks is modeling the unbounded soil. A number of analytical approaches have defined the soil reactions as the functions of excitement frequency. The soil-structure interaction, however, is liable to be affected by non-linear features of the surrounding soil to a great extent, and thus, the actual problems to be solved often exceed the bound of frequency-domain analysis. Extracting the representative features of wave propagation would contribute to simplify the expression of soil reactions. Novak, Nogami and Abouli-Ella (1977) have presented the frequency-domain solutions of soil reactions to the harmonic motion of an embedded cylindrical body limited to cases that can be viewed as plane strain condition. Nogami and Konagai (1986, 1987,1988) have successfully transformed these solutions, in terms of frequency-independent parameters like springs and dashpots, into the time-domain expression which have been applied to the analysis of both the linear and nonlinear transient response of pile foundations. The

validity of the time-domain expression has been also examined through the course of experiments on model piles embedded in a synthetic ground model (Konagai and Nogami, 1994).

In reality, however, soil is not a continuous mono-phase material but consists of the porous granular fabric partly-permeated or perfectly-saturated by water. Therefore, it is quite probable for the soil to show different behavior during earthquakes from the mono-phase continuous material. This paper extends the time-domain expression of soil reaction (Nogami and Konagai, 1988) so that the solid-fluid interaction is rationally taken into account. In the present approach, the model parameters are to be expressed as functions of equivalent Poisson's ratio, that varies with the bulk moduli of fluid and solid phases, permeability and porosity of soil. The present impedance functions for various vibration modes are then attached to the upright beam of Timoshenko type, which represents a flexural embedded body like a pile group, and numerical examples are presented taking porous soil profiles from Kobe as examples.

POROUS SOIL-STRUCTURE INTERACTION FORCE

Based on Biot's theory and using axisymmetric displacement-potential form, the displacements of porous medium in terms of the solid phase displacement and the relative displacement of fluid phase are written in the cylindrical coordinates as:

$$\{u,w\} = \{(u_r,u_z),(w_r,w_z)\} = \{(\nabla\phi + \nabla * \nabla * (\psi i_3)),(\nabla H + \nabla * \nabla * (G i_3))\} \tag{1}$$

where, u_r, u_z= radial and vertical displacements of solid phase, respectively. w_r,w_z= radial and vertical relative displacements of fluid phase with respect to the solid Phase, respectively, ∇ = gradient and i_3 = a unit base vector along z axis. ϕ, H = the potentials of the displacement of solid phase, ψ, G = the potentials of the relative displacement between the solid and fluid phases. The variations of ϕ, ψ are associated with volumetric wave propagation, whereas H, G show distortional wave propagation. Eq.(1) can be rewritten as:

$$\begin{bmatrix} \lambda^* + 2\mu^* + Q & Q \\ Q & Q \end{bmatrix} \nabla^2 \begin{Bmatrix} \phi \\ \psi \end{Bmatrix} = \begin{bmatrix} \rho & \rho_f \\ \rho_f & \alpha\rho_f / n \end{bmatrix} \frac{\partial^2}{\partial^2 t} \begin{Bmatrix} \phi \\ \psi \end{Bmatrix} + \begin{bmatrix} 0 & 0 \\ 0 & b \end{bmatrix} \frac{\partial}{\partial t} \begin{Bmatrix} \phi \\ \psi \end{Bmatrix}$$
$$\begin{bmatrix} \mu^* & 0 \\ 0 & 0 \end{bmatrix} \nabla^2 \begin{Bmatrix} H \\ G \end{Bmatrix} = \begin{bmatrix} \rho & \rho_f \\ \rho_f & \alpha\rho_f / n \end{bmatrix} \frac{\partial^2}{\partial^2 t} \begin{Bmatrix} H \\ G \end{Bmatrix} + \begin{bmatrix} 0 & 0 \\ 0 & b \end{bmatrix} \frac{\partial}{\partial t} \begin{Bmatrix} H \\ G \end{Bmatrix} \tag{2), (3}$$

where, $\lambda^*=\lambda(1+i(da))$, $\mu^*=\mu(1+i(da))$, λ and μ = Lame's constants, da = hysteresis damping ratio of solid phase, $\rho=(1-n)\rho_s+n\rho_f$= density of soil, ρ_s = density of solid, ρ_f= density of fluid, n=porosity, p = atmospheric pressure, $Q=1/(n(1/k_f+(1-s)/p))$, k_f= bulk modules of fluid, s = degree of saturation, $\alpha=2/n-1$= toruosity for spherical shapes, showing mass coupling effect of phases, $b=gn\rho_f/k$= diffusive coefficient, g = gravitational acceleration and k = permeability coefficient of soil.

Obtaining the eigen values and eigen vectors of Eq. (2) allows Eq. (2) to be decoupled with respect to both ϕ and ψ. The solutions of potentials H_1, H_2, ϕ and ψ, G are then obtained as:

$$H_1 = K_m(i\beta_3 r)(C_0 \sin m\theta + C_1 \cos m\theta)\exp(i\omega t) \tag{4-1}$$
$$H_2 = K_m(i\beta_3 r)(C_2 \sin m\theta + C_3 \cos m\theta)\exp(i\omega t) \tag{4-2}$$
$$G_j = \frac{\rho_f}{(ib/\omega - (1/n + \alpha - 1)\rho_f)} H_j \tag{4-3}$$
$$\varphi = (A_1 \sin m\theta + A_2 \cos m\theta)K_m(i\beta_1 r) + (B_1 \sin m\theta + B_2 \cos m\theta)K_m(i\beta_2 r) \tag{5-1}$$
$$\psi = (A_3 \sin m\theta + A_4 \cos m\theta)K_m(i\beta_1 r) + (B_3 \sin m\theta + B_4 \cos m\theta)K_m(i\beta_2 r) \tag{5-2}$$

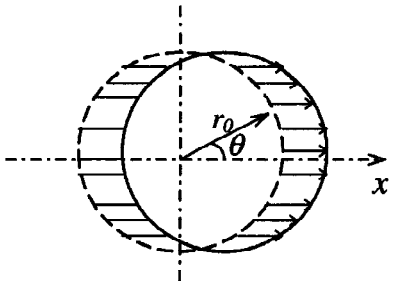

Fig. 1. Swaying motion

where $\beta_j = \frac{\omega}{v_p^*}\lambda_j$ $(j=1,2)$, $\beta_3 = \frac{\omega}{v_s^*}\lambda_3$, K_m=the second modified complex Bessel function of order m, λ_j= the eigen values of Eq.(2), A_i, B_i, C_i = unknown constants, which are to be determined from the boundary conditions. Given the boundary conditions for a rigid disk embedded in a plane strain medium with an infinite extent, the impedance functions for various vibration modes are analytically available (Noorzad and Konagai, 1993). The impedance for swaying motion (Fig. 1) is expressed in the following form as:

$$K_h = \pi\mu(a_3^*)^2 \frac{R_2}{R_3} \tag{6}$$

where, $a_j^* = i\beta_j r_0$, $(j=1,2,3)$,

$$R_2 = K_1(a_3^*)(4K_1(a_1^*) + a_1^* K_0(a_1^*) + 4R_1K_1(a_2^*) + R_1 a_2^* K_0(a_2^*)) + a_3^* K_0(a_3^*)(K_1(a_1^*) + R_1K_1(a_2^*))$$

$$R_3 = a_3^* K_0(a_3^*)(K_1(a_1^*) + R_1K_1(a_2^*) + a_1^* K_0(a_1^*) + R_1 a_2^* K_0(a_2^*)) + K_1(a_3^*)(a_1^* K_0(a_1^*) + R_1 a_2^* K_0(a_2^*))$$

$$R_1 = \begin{cases} \dfrac{(1+t_{21})\beta_1^2 K_1(i\beta_1 r)}{(1+t_{22})\beta_2^2 K_1(i\beta_2 r)} A_2 & \text{For the drained condition} \\ \dfrac{t_{21}\beta_1^2 K_1(i\beta_1 r)}{t_{22}\beta_2^2 K_1(i\beta_2 r)} A_2 & \text{For the undrained condition} \end{cases}$$

The variation of stiffness ratio (k_h/μ) with respect to both the normalized frequency a_0 and the permeability coefficient k is shown in Fig. 2. The real part of the stiffness is getting more and more downward to the right as the permeability coefficient decreases, whereas the imaginary part is less affected by the change in the permeability.

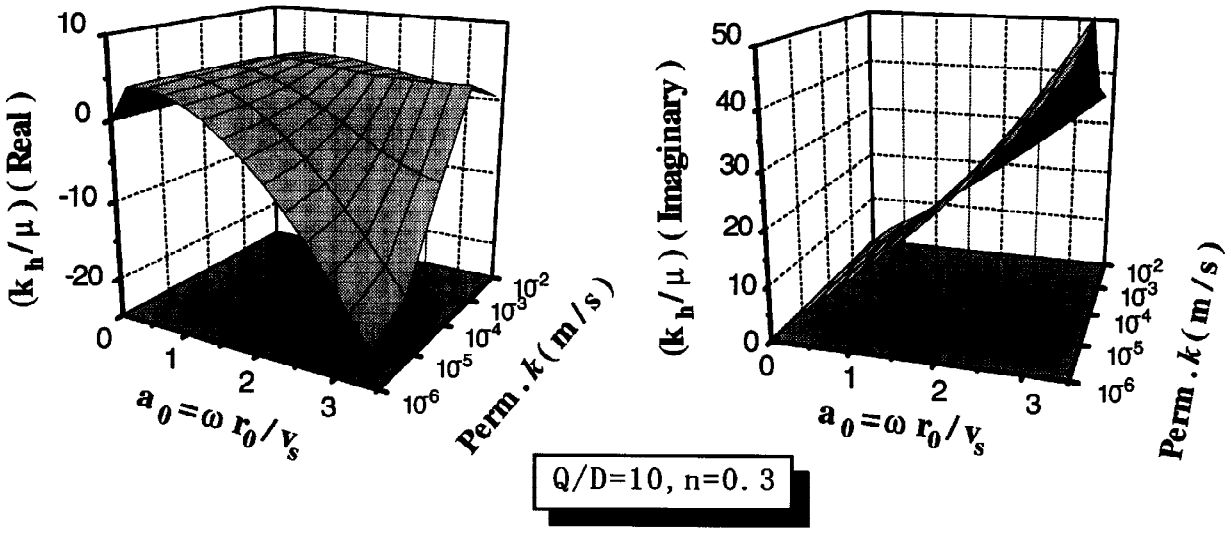

Fig. 2. Variation of the stiffness of porous medium for swaying motion with dimensionless frequency and permeability, the bulk modulus of solid phase D=2.0×10^{4}tf/m^2 and fluid phase Q=2.0×10^{5}tf/m^2, the mass density of solid phase ρ_s=2.6t/m^3 and the coefficient of hysteresis damping da=0.

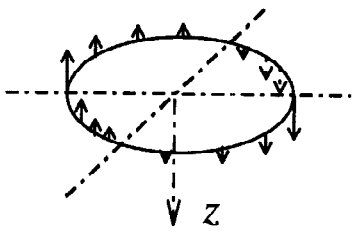

Fig. 3. Rocking motion

The impedance function for rocking motion (Fig. 3) is given as:

$$K_{rp} = \pi\mu r^2(1 + da)(1 + a_3^* \frac{K_0(a_3^*)}{K_1(a_3^*)}) \quad (7)$$

Fig. 4 shows the variation of the rocking stiffness with respect to the normalized frequency and the permeability coefficient. Differing from the case of horizontal motion, both the real and imaginary parts vary slightly with the permeability coefficient. Fig. 2, when compared with Fig. 4, implies that the effect of permeability on the impedance variation appears when the volumetric deformation is accompanied by the wave radiation, because the coupling between the solid and fluid phases affects the pore pressure generation. For this reason, the effect of pore pressure generation can be discussed in the time-domain only when the volumetric wave exists.

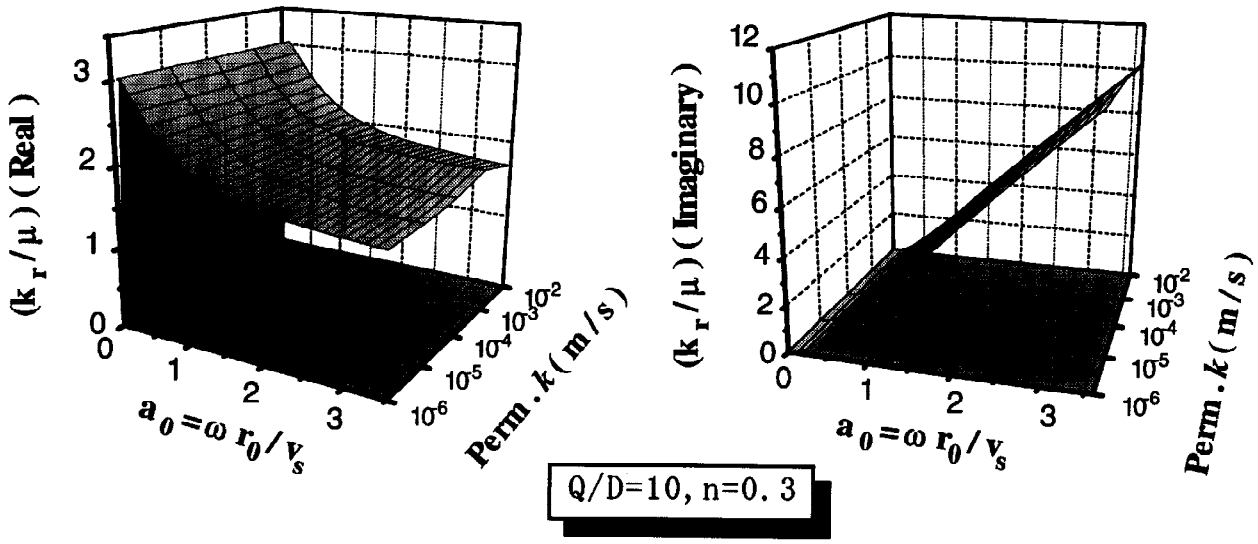

Fig. 4. Variation of the stiffness of porous medium for rocking motion with dimensionless frequency and permeability

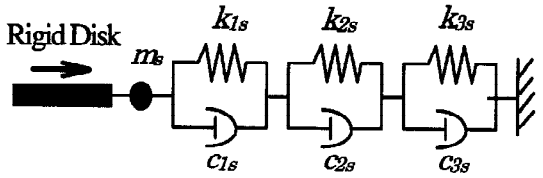

$$k_h(\omega) = \mu\xi_k(v_E)\left(\sum_j \frac{1}{\bar{k}_j + i\bar{c}_j a_0}\right)^{-1} - \mu\xi_m(v_E)a_0^2$$

Fig. 5. Soil model for swaying motion

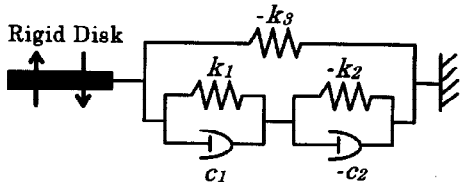

$$k(\omega) = \frac{k_1k_2 - k_3(k_2 - k_1) + \{k_1c_2 + k_2c_1 - k_3(c_2 - c_1)\}a_0 - c_1c_2a_0^2}{(k_2 - k_1) + (c_2 - c_1)a_0}$$

Fig. 6. Soil model for rocking motion

Since the analytical form of the above-mentioned impedance functions are still hard to be directly transformed into the time-domain expressions, the method for modeling impedance functions in terms of frequency-independent parameters (Nogami and Konagai, 1988) is used in the present approach. According to the approach taken by Nogami and Konagai, the reaction to the dynamic lateral motion of an embedded massless disk is well approximated by a synthesis of a couple of Voigt models arranged in series with an added mass at the end (Fig. 5), and three voigt models allows the precise approximation to be obtained within the frequency range, $0.02<a_0<10$. Concerning the rocking motion of the embedded disk, Konagai (1995) also showed that the approximate impedance function of the disk in the frequency domain (Nogami and Sun) is well

approximated by the synthesis of springs and dashpots illustrated in Fig 6. The spring constants, damping constants of the dashpots and the added mass for the models are frequency-independent, and the functions of Poisson's ratio when the motion of disk generates volumetric waves. Therefore, it would be plausible to think over the possibility of incorporating the effect of pore-pressure generation just by introducing the equivalent Poisson's ratio as the function of the bulk moduli of solid and fluid phases, permeability and porosity of soil.

The properties of solid phase are expressed in terms of five parameters: n, G_s, k, λ *and* μ, and two parameters s and p are necessary for describing the fluid phase. The bulk modulus Q of water entrapping air bubbles is noticeably reduced when compared with the state of perfect saturation, and the modulus depends strongly on the degree of saturation. Reviewing some soil profiles along the elevated section of the Hanshin expressway, Kobe, that suffered the devastating damage by the Jan. 17 earthquake of 1995, parameters for describing the three typical soils are set at the values listed in Table 1, where $D=\lambda+2\mu$.

Table 1. Approximate values for parameters of some typical soils in the area of Kobe

Soil type	Porosity n	ρ_s (g/cm^3)	k (m/s)	Q/D (s=0.95)	Q/D (s=1.0)
Diluvial sand or gravel	0.15-0.45	2.6-2.7	10^{-2}-10^{-4}	0.0082	8.99
Alluvial sand	0.2-0.5	2.6-2.7	10^{-2}-10^{-6}	0.036	39.6
Silt or alluvial clay	0.3-0.55	2.5-3.1	10^{-8}-10^{-10}	5.66	6180

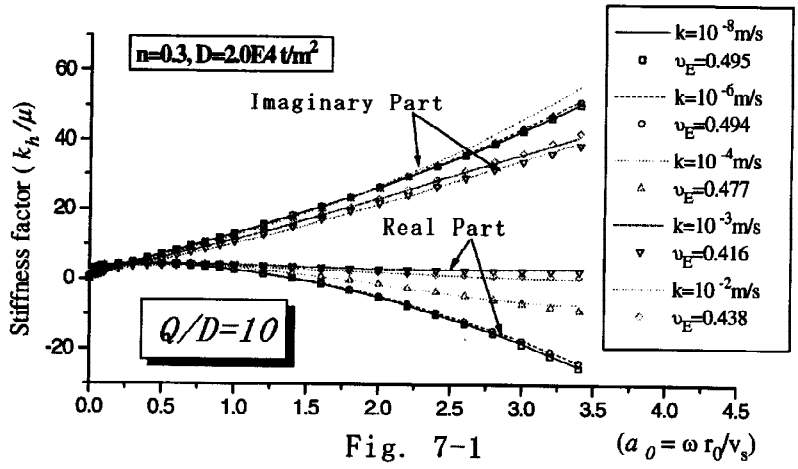

Fig. 7-1

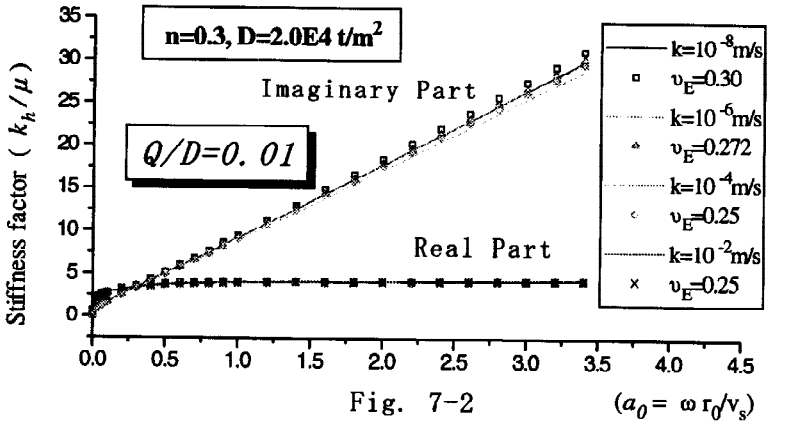

Fig. 7-2

Fig. 7. Comparison of the stiffness calculated by the model of porous medium and the model of continuous medium with equivalent Poisson's ratio

Figs. 7-1 and 7-2 show the variations with frequency of both real and imaginary parts of the horizontal impedance functions for different values of permeability coefficients, setting the other parameters at the prescribed values (n = 0.3, Q/D = 10, D = 2.0×10^4 t/m^2). The open marks are the approximate solutions by the present approach. The best fit to the rigorous solutions is obtained setting the equivalent Poisson's ratios at the values in the legend. The equivalent Poisson's ratio increases as the permeability decreases. On the other hand, the change in the permeability affects little the equivalent Poisson's ratio when the bulk modulus of the fluid phase is low (Fig. 7-2).

Fig. 7-1 offers an important revelation that it is quite possible that the equivalent Poisson's ratio for a completely saturated soil is much smaller than the one from the PS logging. It is not seldom that the PS logging provides the measured longitudinal wave velocity of about

1500m/s, which is equal to the velocity of the sound through water, thus yielding the Poisson's ratio of about 0.5. As is shown in the figure, the higher the normalized frequency is, the clearer the effect of Poisson's ratio on the impedance function is. Therefore the soil parameters must be carefully determined especially when a thick foundation with a large representative size is embedded in a water-saturated loose sandy soil deposit with comparatively high permeability.

TRANSFER MATRIX APPROACH FOR EMBEDDED TIMOSHENKO BEAM

When an embedded body is a flexible structure like a slender caisson or a pile group, the beam of Timoshenko type would be preferable to the one of Beronoulli-Euller type for the model of the embedded body. Differing from the model of Beronoulli-Euller beam which only considers the deformation contributed by bending, the deformation in the model of Timoshenko beam is associated with both bending and shearing. Governing equations of a Timoshenko beam supported by the soil springs of Winkler type are given as:

$$\rho A\frac{\partial^2(u_b+u_s)}{\partial t^2}=GA\frac{\partial^2 u_s}{\partial x^2}-p_s(z)$$
$$\rho I\frac{\partial^2\varphi_b}{\partial t^2}=EI\frac{\partial^2\varphi_b}{\partial x^2}+GA\frac{\partial u_s}{\partial x}-p_b(z) \qquad \text{(8-1), (8-2)}$$

where, u_b, u_s = the lateral deformations due to bending and shearing, respectively. $\varphi_b=\partial u_b/\partial z$, p_s and p_b are the lateral reaction force and moment of soil for swaying and rocking motion, respectively. The formulae shown in Fig. 5 and Fig. 6 are used to express the reaction forces p_s and p_b, respectively. According to the Winkler's hypothesis, p_s and p_b are determined only by the displacement at the depth z. The loading time history is digitized at time increment Δt. In the step-by-step analysis, p_s and p_b at time t_i is expressed as:

$$p_{s,i}=k_s(u_{b,i}+u_{s,i}-u_{g,i})+d_{s,i}$$
$$p_{b,i}=k_b\varphi_{b,i}+d_{\varphi,i} \qquad \text{(9-1), (9-2)}$$

where, $d_{s,i}$ and $d_{\varphi,i}$ are given as constants at t_i , which are determined using known displacements, velocities and accelerations at the previous time step t_{i-1} . By assuming the increment of acceleration is proportional to $(t-t_{i-1})^{\alpha}$, the accelerations $\ddot{u}_{b,i}$, $\ddot{u}_{s,i}$ and $\ddot{\varphi}_{b,i}$ can be expressed as:

$$\ddot{u}_{b,i}=\xi_a u_{b.i}-\zeta^a_{b,i}$$
$$\ddot{u}_{s,i}=\xi_a u_{s.i}-\zeta^a_{s,i} \qquad \text{(10-1), (10-2), (10-3)}$$
$$\ddot{\varphi}_{b,i}=\xi_a \varphi_{b.i}-\zeta^a_{\varphi,i}$$

where, $\xi_a=\dfrac{(\alpha+1)(\alpha+2)}{\Delta t^2}$, $\zeta^a_{b,i}$, $\zeta^a_{s,i}$ and $\zeta^a_{\varphi,i}$ are the functions of displacements, velocities and accelerations at the previous time step, respectively (Nogami and Konagai, 1986). Substituting Eqs. (9-1), (9-2), (10-1)-(10-3) into Eqs. (8-1), (8-2), the following equations are obtained:

$$\rho A\{\xi_a(u_{b,i}+u_{s,i})-\zeta^a_{b,i}-\zeta^a_{s,i}\}=GA\frac{d^2u_{s,i}}{dx^2}-\{k_s(u_{b,i}+u_{s,i}-u_{g,i})+d_{s,i}\}$$
$$\rho I(\xi_a\frac{du_{b,i}}{dx}-\zeta^a_{\varphi,i})=EI\frac{d^3u_{b,i}}{dx^3}+GA\frac{du_{s,i}}{dx}-(k_b\frac{du_{b,i}}{dx}+d_{\varphi,i}) \qquad \text{(11-1), (11-2)}$$

Both the displacements $u_{s,i}$ and $u_{b,i}$ within a segment are assumed to be expressed in polynomial form as:

$$u_{s,i}=C_{s3,i}x^3+C_{s2,i}x^2+C_{s1,i}x+C_{s0,i}$$
$$u_{b,i}=C_{b4,i}x^4+C_{b3,i}x^3+C_{b2,i}x^2+C_{b1,i}x+C_{b0,i} \qquad \text{(12-1), (12-2)}$$

There are 9 unknown constants ($C_{sj,i}$ and $C_{bj,i}$) in the above equations. In the transfer matrix approach, 5 physical quantities are transferred from one end of the segment to another. They are: *(1)* displacement due to swaying $u_{s,i}$, *(2)* displacement due to rocking $u_{b,i}$, *(3)* rotation angle $\varphi_{b,i}$, *(4)* shear force $GA(du_{s,i}/dz)$ and *(5)* moment $EI(d^2u_{b,i}/dx^2)$. These quantities are given at the both ends of the segment. Therefore, the total 10 quantities are expressed in terms of the 9 unknown constants by using Eqs. (12-1), (12-2). Moreover, the

governing equations (11-1), (11-2) should be satisfied at the both ends of the segment, that is, another 4 equations are added. As the consequence, total 14 equations are available. Hence, any 9 equations out of these 14 are used to determine the 9 unknown constants and, the transfer matrix can be formulated by using another 5 equations left. After building up the transfer matrixes, there are 10 unknown quantities on the top and bottom ends of the beam. Therefore, 5 boundary conditions are seemingly needed to be given in the process of step-by-step computation. However, it is noted that either or both of $u_{b,i}(z)$ and $u_{s,i}(z)$ could be shifted to any extent as far as the displacement compatibility is satisfied at the boundaries. In other words for example, it would be possible to replace $u_{b,i}(z)$ with $u_{b,i}(z)+B_i$ so that the bottom displacement $u_{b,i}(z_{bottom})+B_i$ is equal to any arbitrarily chosen constant C. Thus, only 4 boundary conditions are needed.

NUMERICAL EXAMPLES

An embedded cylinder shown in Fig. 8 with an inverted pendulum on its top is considered. Two extreme cases of soil profiles are set up within the possible extents of parameters for the soils shown in Fig. 8. Case 1 premises the presence of the comparatively impermeable sandy soil fill, probably with finer grains mixed in, over the subsurface alluvial clay, whereas a permeable soil fill overlies the subsurface material in case 2.

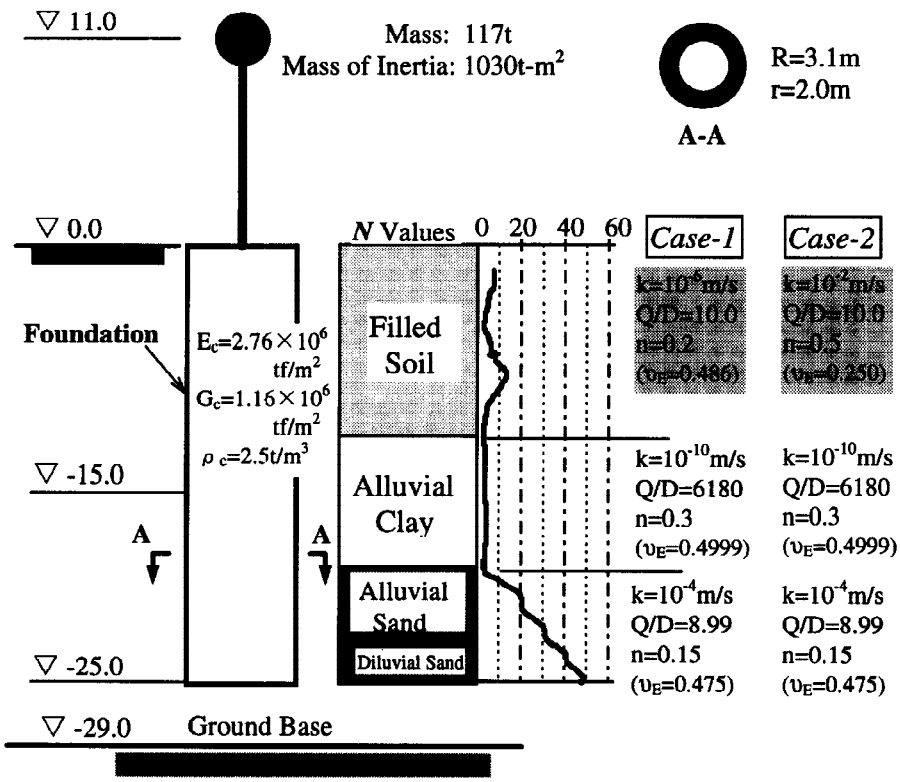

Fig. 8. The sketch of the foundation with the soil profile

The acceleration time history recorded at the Kobe Marine Meteorological Observatory, Jan. 17, 1995, is input, through a dashpot, to the stiffer soil layer beneath the depth of embedment (-29m). The dashpot represents the effect of energy dissipation by the waves going down into an infinite extent. The acceleration time history, in which the peak value of 818cm/s^2 has been reached, is noticeably strong enough for the nonlinear response analysis to be indispensable. In the first place, however, the time-domain soil-foundation interaction is discussed in terms of linear elasticity for the solid phase, even though the present approach has the capability of incorporating nonlinear behavior of porous medium. The subject of discussion is thus the effect of the permeability of soil on the dynamic response of the soil-structure system.

Fig. 9 shows the time histories of the relative displacement of the pendulum mass to the motion of the base layer beneath the embedment depth (-25m). It is clear from the figure that about 30% reduction of the peak values of displacement in case 1 is due to the decrease of the permeability of the surface soil fill. The effect of the permeability is much clearer at the level of the foundation top (0.0m). It is also noted in this figure that the time histories at different levels (the foundation top and the middle depth of embedment (-15m)) are out of phases each other. the numerical result have shown that the embedded body has the sharpest bent at the middle depth (-11m).

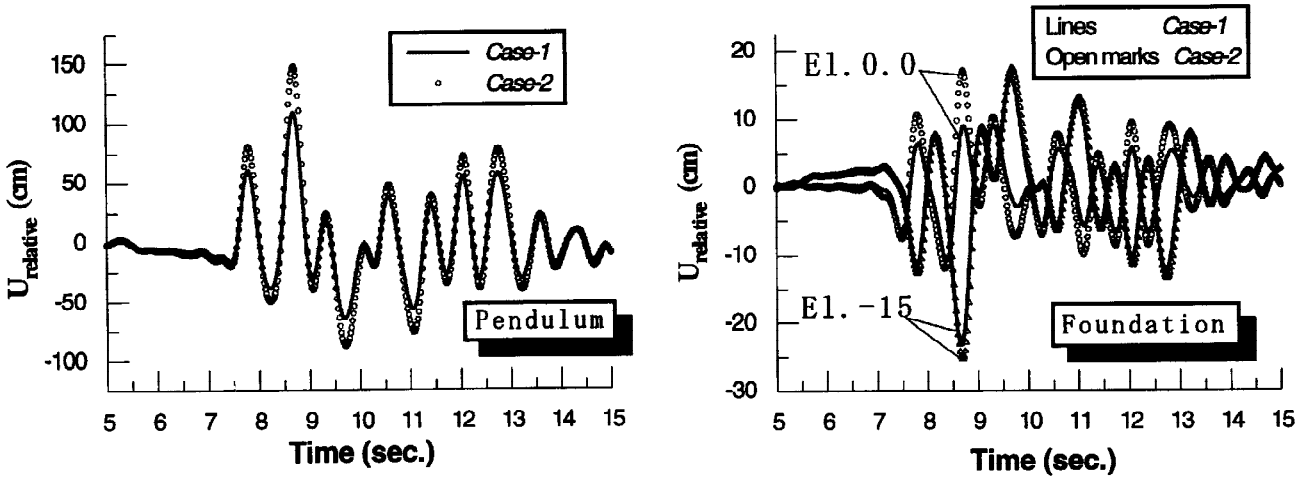

Fig. 9. Relative displacements of the structure

CONCLUSIONS

A simple model for analyzing the porous soil-structure interaction has been developed. In the present approach, the porous soil medium surrounding the foundation of interest is sliced into a number of elements. Grasping the typical patterns of wave radiation through the sliced elements, the impedance functions for various vibration modes of the embedded disk are approximated by the syntheses of springs and dashpots. Since the springs and dashpots are independent of the excitement frequency, the present model is capable of analyzing the time-domain response of porous soil-structure systems. The frequency-independent parameters for the soil model are the functions of the equivalent Poisson's ratio, and it is probable for the equivalent Poisson's ratio to be quite different from the one obtained through the in-situ PS logging. The difference is much more pronounced when a water-saturated rather coarse sandy soil deposit with comparatively high permeability is concerned. Assuming the case in which the surface soil layer of this sort overlies the subsurface material, the dynamic response of an inverted pendulum on an embedded upright Timoshenko beam is examined. Change in permeability of the surface soil within a possible range (10^{-6}m/s<k<10^{-2}) yielded a noticeable difference of the structure because the stiffness of the very surface layer has the greatest influence on the response of the structure.

REFERENCES

Novak, M., T. Nogami and F. Abouli-Ella (1978). Dynamic soil reactions for plane strain case, *J. eng. mech.* ASCE, **104**, 953-959.

Nogami, T. and K.Konagai (1986). Time-domain axial response of dynamically loaded single piles, *J. eng. mech.* ASCE,**112**, 1241-1252.

Konagai, T. and T.Nogami (1987). Time-domain axial response of dynamically loaded pile groups, *J. eng. mech.* ASCE, **113**, 417-430.

Nogami, T. and K.Konagai (1988). Time-domain flexural response of dynamically loaded single piles, *J. eng. mech.* ASCE, **114**, 1512-1525.

Konagai, K. and T.Nogami (1994). Subgrade model for transient response analysis of multiple embedded bodies, *Earthquake eng. struct. dyn.* **23**, 1097-1114.

Noorzad, A. and K. Konagai (1993). Comparison between resistances of porous and continuous model of saturated soil for plain strain case, *"SEISAN-KENKYU"*, I.I.S., University of Tokyo, **45**, 567-569.

Konagai, K. (1995). Simplified time-domain expression of soil response to transient loading, *Research report to Norwegian Institute of Technology, University of Trondheim,* Trondheim, Norway, 1-21.